



Article

Characterization of Three Surges of the Kyagar Glacier, Karakoram

Zhen Zhang ^{1,*} , Jinbiao Zhao ¹, Shiyin Liu ² , Qibing Zhang ³, Zongli Jiang ⁴, Yangyang Xu ¹ and Haoran Su ⁵¹ School of Geomatics, Anhui University of Science and Technology, Huainan 232001, China² Institute of International Rivers and Eco-security, Yunnan University, Kunming 650091, China³ College of Geography and Tourism, Hunan University of Arts and Science, Changde 415000, China⁴ School of Earth Sciences and Spatial Information Engineering, Hunan University of Science and Technology, Xiangtan 411201, China⁵ School of Architecture, Harbin Institute of Technology (Shenzhen), Shenzhen 518055, China

* Correspondence: zhangzhen@aust.edu.cn

Abstract: Glaciers experience periodic variations in flow velocity called surges, each of which influences the glacier's characteristics and the occurrence of downstream disasters (e.g., ice-dammed lake outburst floods). The Karakoram region contains many surging glaciers, yet there are few comprehensive studies of multiple surge cycles. In this work, Landsat, topographic map, Shuttle Radar Topography Mission (SRTM), TerraSAR-X/TanDEM-X, ITS_LIVE, and Sentinel-1 glacier velocity data were used to systematically analyze the characteristics of Kyagar Glacier since the 1970s. Three surging events were identified, with active phases in 1975–1978, 1995–1997, and 2014–2016. The timing of these surges was similar, with a cycle of 19–20 years, an active phase of 3–4 years, and a quiescent phase of 16–17 years. During the quiescent phase, a large amount of ice accumulates in the lower part of the accumulation zone, and the terminal of the tongue thins significantly. According to the most recent surge event (2014–2016), glacier flow accelerated suddenly in the active phase and reached a maximum velocity of $2 \pm 0.08 \text{ m d}^{-1}$. Then, the glacier terminal thickened sharply, the reservoir zone thinned by $12 \pm 0.2 \text{ m}$, and the terminal receiving zone thickened by $28 \pm 0.2 \text{ m}$. The glacier may have entered a quiescent phase after July 2016. The glacier surge causes a large amount of material to transfer from upstream to downstream, forming an ice dam and creating conditions for a glacial lake outburst flood (GLOF). At the termination of the active phase, the subglacial drainage channel became effective, triggering the GLOF. For a period of the quiescent phase, the glacier ablation intensifies and the GLOF repeats constantly. One surge caused 7–8 GLOFs, and then a continuous reduction in the ice dam elevation. Eventually, the ice dam disappeared, and the GLOF no longer continued before the next glacier-surfing event.

Keywords: glacier surging; glacial lake outburst; Karakoram; remote sensing

Citation: Zhang, Z.; Zhao, J.; Liu, S.; Zhang, Q.; Jiang, Z.; Xu, Y.; Su, H. Characterization of Three Surges of the Kyagar Glacier, Karakoram. *Remote Sens.* **2023**, *15*, 2113. <https://doi.org/10.3390/rs15082113>

Academic Editors: Ulrich Kamp and Gareth Rees

Received: 2 March 2023

Revised: 7 April 2023

Accepted: 14 April 2023

Published: 17 April 2023



Copyright: © 2023 by the authors. Licensee MDPI, Basel, Switzerland. This article is an open access article distributed under the terms and conditions of the Creative Commons Attribution (CC BY) license (<https://creativecommons.org/licenses/by/4.0/>).

1. Introduction

Surging glaciers are characterized by quasi-periodic changes between periods of fast (active phase) and slow flow velocities (quiescent phase) [1]. A surging cycle is divided into two phases: the active and quiescent phases [2]. During an active phase, the flow velocity can be 10–1000 times greater than in the quiescent phase, thus causing rapid mass transfer from the reservoir zone to the receiving zone, which can even result in a frontal advance [3]. Meanwhile, natural disaster events caused by glacier surging can greatly threaten downstream areas, such as glacial lake outburst floods (GLOFs), glacial meltwater debris flows, and glacier collapses [4–6]. Therefore, studying the dynamics of surging glaciers can help predict glacier behavior and hazard development.

About 1% of the world's glaciers are surging glaciers, which have a clustered distribution and mainly occur in High-Mountain Asia (HMA) and the high latitudes of the Arctic (from Alaska, Novaya Zemlya, and Svalbard to Greenland); [7]. There are also a number of surging glaciers in other parts of the world, such as the Andes [8]. As HMA is the birthplace of many great rivers, its future development of glaciers is of great concern [9].

Glaciers in HMA have decreased significantly in mass under global warming [10]. However, glaciers in some areas, such as Pamir, the Karakoram Mountains, and West Kunlun, have shown stable/advanced or weakly positive mass balances [11,12], which is a part of the “Karakoram anomaly” [13]. Historically, Karakoram glacier surges have been widely recorded, with at least 220 glaciers reported to do so. These surges do not appear to be dependent on climate change [14]. Therefore, in order to better understand the Karakoram glacier changes, we need to strengthen the monitoring of the glacier surging.

The surface features of a surging glacier change dramatically during its development, which facilitate their detection by remote sensing. We have to underline that remote sensing plays an important role in the study of surging glaciers, which is mainly used to monitor the flow velocity, elevation change, and surface change of glaciers [6,8,14–24]. At present, the remote sensing works in the literature on the surface velocities of glaciers include two methods: Feature Tracking and Synthetic Aperture Radar Interferometry (InSAR) [14,17,22]. The rapid changes of the glacier’s surface during the glacier surge often result in incoherence between Synthetic Aperture Radar (SAR) images, which renders it difficult to extract the velocity effectively by the InSAR method [14,17,22]. Therefore, for SAR images, the glacier velocity is also extracted by Feature Tracking [25]. The Digital Elevation Model (DEM) is mainly used to explore the surface elevation change of the surging glacier [23,24]. Currently, there are two main methods for DEM extraction based on remote sensing, namely stereo remote sensing photogrammetry and InSAR, which both play an important role in examining the glaciers’ properties [10–12].

There are many studies on glacier surging in the Karakoram, mainly comprising surging glacier inventories [14,15] and analyses of individual (or several) glaciers [16–18]. Most detection and analysis of surging glaciers are based on remote sensing methods according to changes in their morphology, velocity, elevation, and other factors [19–21]. In particular, glacier velocity data extracted from optical and radar remote sensing images play an important role in the study of surging glaciers [16,22]. A glacier can be determined to be surging due to unusual changes in its velocity, and the dynamics of glacier surging can be analyzed using velocity time series [23,24]. Remote sensing image data (e.g., Landsat TM) relevant to glacier velocity sequences became available in the 1990s. However, due to the effects of clouds and snow, it can be very difficult to obtain a long, complete time series. In addition, in the past, it was difficult to obtain glacier velocity time series on a monthly scale; however, in recent years, Sentinel-1 data have provided good data for this purpose [25]. Elevation changes can be detected by multi-period Digital Elevation Model (DEM) subtraction or radar interferometry while surging glaciers can be identified based on elevation changes in their reservoir and receiving zones. However, it is difficult to obtain elevation-change data before the year 2000, so a few studies employ topographic maps or DEMs extracted from spy satellites (such as Corona and Hexagon) to identify surging glaciers [23]. As remote sensing is a relatively new technology, suitable data have only become abundant after 2000 [26]. As some glacier surge cycles are likely to last longer than 50 years, more than two surge events can rarely be observed on the same glacier by remote sensing [19]. The Karakoram region contains some glaciers that repeatedly surge and, although these processes have been documented [14,19], few studies have focused on multiple surges in a particular glacier.

Karakoram GLOF events are very frequent and many are associated with glacier surging [27]. However, the dynamic process of GLOFs caused by glacier surging is still not well understood [24]. Hence, it is very important to clarify the relationship between surging behavior and GLOF disasters. The Kyagar Glacier (Figure 1), located on the northern slope of the Karakoram Range, has been a site of several GLOF events that have caused severe damage in the lower reaches of the Yarkand River [28]. Although the Kyagar Glacier showed signs of advancing in the 1920s, 1970s, and 1990s [29], it was not identified as a surging glacier until a surge in the year 2014–2015 was reported by Round et al. [30]. Bhambri et al. [14] confirmed that the glacier surged in the 1990s, the details of which were not reported.

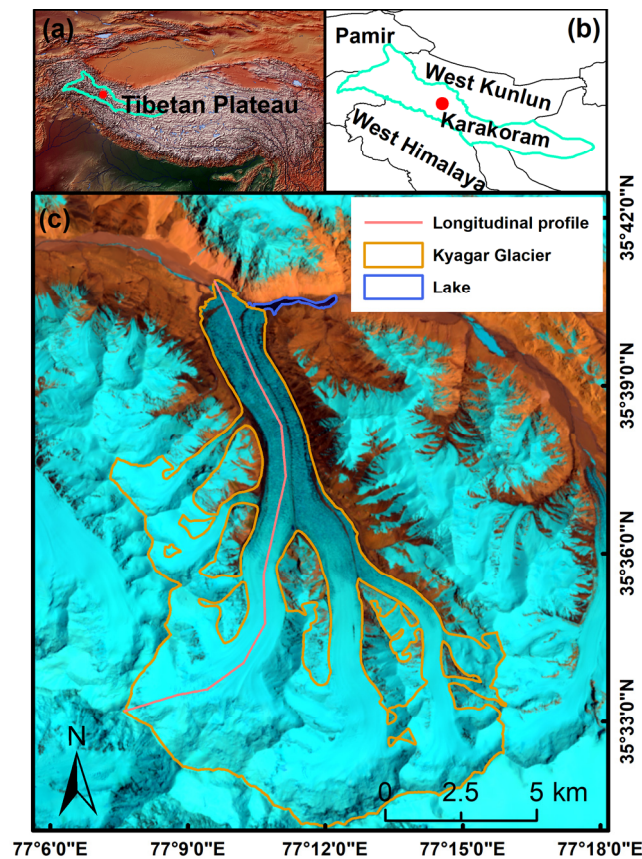


Figure 1. Kyagar Glacier. Location within the (a) Tibetan Plateau and (b) Karakoram Mountains. (c) Landsat image from 4 July 2015. The pink line indicates the position of a longitudinal profile used to analyze glacier velocity and elevation changes.

To enhance the understanding of the surge dynamics of Kyagar Glacier and the relationship between surges and GLOFs, this study identified three surges of Kyagar Glacier since the 1970s using Landsat data, glacier velocities extracted from optical and radar remote sensing images, topographic maps, Shuttle Radar Topography Mission (SRTM), and TerraSAR-X/TanDEM-X. The relationship between surges and GLOFs was analyzed, and the surging period and process were established.

The rest of this work is structured as follows: In Section 2, the general situation of the study area is described. The data and method are analyzed in detail in Section 3. In Section 4, the glacier surging process is described, and in Section 5, our results from the methodological and glaciological perspectives are discussed, respectively. Finally, the conclusions of our work are drawn in Section 6.

2. Study Site

The Kyagar Glacier (Figure 1) is a polythermal valley glacier located in the Karakoram Mountains in the southeast of the Xinjiang Uygur Autonomous Region. Its elevation ranges from 4759 m to 7186 m, with a total area of about 95 km², an average surface slope of 22°, and an average aspect of 37.2°. It is composed of three tributaries ranging from 6 km to 10 km in length, which converge to form an ice tongue 8 km long and about 1.5 km wide. The north–south Kyagar Glacier blocks the east–west Shaksgam Valley, creating a glacial lake that, if it did outburst, would flood the downstream Yarkand River. The region is dominated by westerlies, with most of the precipitation occurring from May to September and the average annual temperature below 0 °C. The ERA5 data from 1950 to 2019 show that the average temperature in this region is −17.8 °C, and the annual average precipitation is 454 mm.

3. Data and Methods

3.1. Data

3.1.1. Landsat Images

To monitor the surge process of the Kyagar Glacier, we acquired 24 Landsat images from the United States Geological Survey (USGS) taken between 1975 and 2021 (Table 1). These images are all L1T products, and systematic radiometric and geometric corrections were carried out by the USGS as well as orthorectification with a DEM.

Table 1. Overview of data sources.

Data	Acquisition Date	Path/Row	Pixel Size (m)/Scale	Amount	Application
Landsat MSS	1973–1979	159/35	79	9	Glacier and glacial lake boundary identification
Landsat TM	1995–1997	148/35	30	6	
Landsat OLI	2013–2021	147/35, 148/35	15	9	
ITS_LIVE	1989–2018		240	30	Annual glacier velocity
Sentinel-1 glacier velocity data	2014–2021		200	79	Monthly glacier velocity
Topographic map	November 1976		1:50,000	1	Glacier elevation change
SRTM	11–12 February 2000		30	1	
TerraSAR-X /TanDEM-X	28 February 2013		12	6	
	3 February 2014				
	12 October 2015				
	13 July 2016				
	3 August 2017				
	5 September 2017				

3.1.2. Glacier Surface Velocity Data

To evaluate the interannual changes in the velocity of Kyagar Glacier, we acquired the Inter-Mission Time Series of Land Ice Velocity and Elevation (ITS_LIVE) data from NASA. This glacier velocity product is based on Landsat 4, 5, 7, and 8 images and adopts the autonomous Repeat Image Feature Tracking processing scheme described by Gardner et al. [31] to extract glacier velocity through local normalization, over-sampling, and feature tracking. The data have good robustness, and errors may be caused by image matching. However, surge events may be much shorter than a year (e.g., a few months), and a mean annual value will then strongly underestimate real flow velocities. In our study, annual glacier velocity data from 1986 to 2018 were used with a spatial resolution of 240 m.

We also used the glacier velocity product derived from Sentinel-1 radar images described by Friedl et al. [25]. This provides monthly average glacier velocity data since October 2014 with a spatial resolution of 200 m. The product input data are Sentinel-1 data, a type of SAR data that is not affected by cloud and fog. These data do, however, suffer from layover and radar shadow in steep mountain terrain.

3.1.3. TerraSAR-X/TanDEM-X Data

The German radar satellites TerraSAR-X and TanDEM-X, developed by EADS Astrium in conjunction with the German Aerospace Centre, were launched into their intended orbits in 2007 and 2010, respectively [32]. TanDEM-X and TerraSAR-X fly synchronously at a distance of less than 200 m from their orbit to accurately scan the earth's surface. These satellites work in a similar way to human eyes, scanning the entire surface of the earth repeatedly to create a high-precision 3D digital model of the planet. To determine changes in glacier elevation, we used CoSSC (Co-registered Single-look Slant-range Complex) experimental files obtained between 2013 and 2017 under the bistatic InSAR strip-map model (Table 1).

3.1.4. Other Data

The Shuttle Radar Topography Mission (SRTM) DEM and topographic map (1:50,000) were also used to analyze glacier elevation changes. SRTM data were obtained for 11–22 February 2000. We used 1 arc-second (about 30 m)-resolution C-band SRTM DEM [33]. The topographic map was taken by aerial photography in October 1976. The contour distance of the topographic map is 10 m, the vertical accuracy of flat areas (i.e., slopes less than 2°) and hilly areas (i.e., slopes of 2–6°) is better than 3–5 m, and the vertical accuracy of the mountain and high mountain areas (i.e., slopes more than 6°) is better than 8–14 m. We directly obtained digital contour lines from the State Bureau of Surveying and Mapping of China (SBSMC) for DEM production.

In addition, ERA5 reanalysis temperature and precipitation data were used in our study. ERA5 is the fifth generation of European Centre for Medium-Range Weather Forecasts (ECMWF) Atmospheric Reanalysis global climate data. ERA5 will eventually replace ERA-Interim reanalysis data [34].

3.2. Glacier and Lake Parameter Extraction

The glacier boundary was extracted by visual interpretation of Landsat images. To improve accuracy, we extracted glacier boundaries based on the second Chinese Glacier Inventory data [35]. We kept the glacier's upper accumulation area unchanged and only modified the part that changed at the glacier terminus so as to obtain glacier boundaries in different years. The glacier area was extracted directly based on the glacier boundary using ArcGIS software.

The glacier has a middle moraine, which divides the glacier into two ice flows, one flowing to the east and the other to the west. We extracted the basis of the centreline of each ice flow based on Euclidean allocation as described by Zhang et al. [36], while the change in length of the centreline at the glacier terminus was taken as the change in glacier length.

The artificial visual interpretation was used to determine the digitized outlines of the glacial lake in different periods, whilst DEM without a lake as a base was used to extract the glacial lake volume.

3.3. DEM Production and Glacier Elevation Change Estimation

Based on the differential synthetic aperture radar interferometry (DInSAR) method, SRTM DEM and TerraSAR-X/TanDEM-X were used to estimate elevation changes for the periods 2000–2013, 2000–2014, 2000–2015, 2000–2016, 2000–2017 (August), and 2000–2017 (September). First, a bistatic interferogram (TerraSAR-X and TanDEM-X form a dual station for data acquisition) was generated from TerraSAR-X/TanDEM-X data and the SRTM DEM. Then, the topographic phase was removed from the bistatic interferogram and a differential interferogram was generated by using the topographic residual phase. Finally, the difference interferogram was used to obtain the surface elevation changes. Meanwhile, TerraSAR-X/TanDEM-X DEMs for 2013, 2014, 2015, 2016, and August and September 2017 were created using the DInSAR method. A detailed description of the above processes is given in Neckel et al. [37]. These methods can directly obtain the surface elevation changes from 2000 to 2013. The elevation changes during 2013–2014, 2014–2015, 2015–2016, 2016–2017, and August–September 2017 were obtained by subtracting TerraSAR-X/TanDEM-X DEMs for different periods. To further reduce the error caused by matching different DEMs, the universal co-registration method proposed by Nuth and Kääb [38] was used for the correction of matching biases.

Digital contour data were extracted from topographic maps from the SBSMC, which was re-projected to the Xi'an Geodetic Coordinate System 1980. The geoid was based on the 1985 Yellow Sea datum. By using the control points of different coordinate systems provided by the SBSMC, we converted the Xi'an Geodetic Coordinate System 1980 into the World Geodetic System 1984 (WGS84) Universal Transverse Mercator (UTM) projection coordinate system using the seven-parameter method. The elevation datum was also converted to the WGS1984 ellipsoid elevation. Then, the Thiessen polygon method (the adjacent elevation points were connected with triangles, and then vertical bisectors for each

side of the triangle were made; a polygon surrounded by several vertical bisectors around each elevation point was thus formed; the elevation of a polygon region is represented by the elevation value contained in the polygon) was used to interpolate the contour lines into a DEM with a 30 m resolution. We subtracted the gravity anomaly and converted the elevation datum to the 1996 Earth Gravitational Model (EGM96), which is consistent with the SRTM DEM. Finally, the co-registration method (the DEM matching error can be corrected by taking into account the relationship with the slope and aspect) proposed by Nuth and Kääb [38] was used to correct the matching errors between the topographic map DEM and SRTM DEM, and the glacier surface elevation changes from 1976 to 2000 were obtained by subtraction.

3.4. Uncertainties

Here, Section 3.4.1 describes the uncertainty assessment method for glacier length and area, Section 3.4.2 analyzes the uncertainty assessment method for glacier velocity, and Section 3.4.3 deals with the uncertainty assessment method for glacier elevation change.

3.4.1. Uncertainties in the Glacier Length and Area Changes Estimation

Glacier boundary errors include interpretation errors, technical errors, and methodological errors. When we interpret the glacier boundary, a single person interprets the same inventory data as a reference, and only changes are modified, so the interpretation errors can be ignored. The Landsat data were orthorectified by the USGS, and the technical errors were negligible [39]. Therefore, we only considered method errors, which are determined by the spatial resolution of the Landsat images. The centreline error is difficult to evaluate, so we only considered the changes at the glacier terminus. The length uncertainty (E_c) was determined by the uncertainty at the glacier terminus in each phase, assuming this to be half a pixel (ε_1 or ε_2 ; [40]). On the basis of the law of error propagation, E_c was calculated according to Formula (1).

$$E_c = \sqrt{\varepsilon_1^2 + \varepsilon_2^2} \quad (1)$$

The area error can be evaluated as the area of the buffer zone of the glacier boundary with a diameter of half a Landsat pixel. Since we only considered the glacier changes between two periods when interpreting the glacier boundary, in the actual error assessment, we only took the buffer area of the perimeter of the region that did change in each period as ε_1 or ε_2 . Then, Formula (1) was used to obtain E_c : the uncertainty in the change in the glacier area.

3.4.2. Uncertainty in Glacier Velocity Estimation

The ITS_LIVE data provide estimates of glacier velocity error. In the process of ITS_LIVE data production, the velocity of each component is tied to the stable region, and the median of each velocity component (V_x , V_y) is set to zero on the non-glacial region so as to correct for co-registration errors. Velocity components deviating by more than three times the quartile range from the median value of all pixels in the same position are assumed to be gross outliers and are eliminated. The uncertainty in each image-pair velocity value is set as the standard deviation of the component velocity measured in the stable region. The uncertainties in merging velocities are estimated on a pixel basis by propagating the uncertainty of each image-pair velocity, as described by Dehecq et al. [41].

Assuming that the correction successfully eliminates existing co-registration errors during the production of Sentinel-1 velocity data, the remaining velocity error is 0.1 pixels of the tracking accuracy. Therefore, for Sentinel-1 data with a pixel size of 3×14 m, the theoretical velocity errors obtained under 6 d and 12 d repeat cycles are 0.24 m d^{-1} and 0.12 m d^{-1} , respectively. Friedl et al. [25] suggested that the uncertainty in glacier velocity generated by 12 d Sentinel-1 data is lower ($\sim 0.08 \text{ m}^{-1}$).

3.4.3. Uncertainty in Glacier Elevation Change Estimation

We assessed the uncertainty in glacier elevation change using the method of Fischer et al. [42], which was developed by Rolstad et al. [43]. The uncertainty in elevation change (E_{dh}) is derived from Formula (2):

$$E_{dh} = \sigma_{dh} \sqrt{\frac{\pi L^2}{5A_{t1}}} \quad (2)$$

where σ_{dh} is the standard deviation of elevation change in the non-glacial region, A_{t1} is the glacier area at the start of the elevation change period, and L is the spatial autocorrelation length. In our study, the spatial resolution of glacier elevation variation obtained by TerraSAR-X/TanDEM-X is 10 m, and L is 185 m as obtained by Moran's index [44]. As the spatial resolution of glacier elevation changes obtained from topographic maps and SRTM is 30 m, L was set to 600 m.

4. Results

It was found that at least three surges occurred in Kyagar Glacier. In Sections 4.1–4.3, the surges in three stages (1975–1978, 1995–1997, 2014–2016) were described in detail. In Sections 4.4 and 4.5, the velocity and elevation changes of Kyagar Glacier were examined, respectively. Moreover, in Section 4.6, the formation process of the glacial lake in front of Kyagar Glacier was thoroughly investigated.

4.1. Glacier Surging during 1975–1978

According to Landsat MSS images from 1973 to 1979 (Figure 2), the east side of the terminus of the Kyagar Glacier showed signs of advancement in March 1975 (by 200 ± 56 m relative to 1973). From November to December 1976, the glacier advanced again by 82 ± 56 m. The glacier advanced 126 ± 56 (18 ± 8 m/month) from December 1976 to July 1977, indicating that the glacier velocity during this period was lower than in November–December 1976. From 14 July 1977 to 18 July 1978, the glacier continued to advance 37 m. The Landsat image on 7 June 1979 shows that the glacier had already begun to retreat and so it had probably stopped surging in 1978. The glacier velocity probably reached its peak in the winter of 1976.

4.2. Glacier Surging during 1995–1997

According to Landsat images from 1995–1997 (Figure 3), the east side of the terminus of the Kyagar Glacier began to advance in 1995. From January to November 1995, the east side of the terminus of the Kyagar Glacier had advanced 247 ± 21 m, and its area increased by 0.08 ± 0.02 km². From November 1995 to February 1996, the east side of the terminus of the glacier continued to advance by 87 ± 21 m, and the area expanded by 0.08 ± 0.02 km². From February to August 1996, there was little change in the east side of the terminus position; however, the west side advanced 75 ± 21 m, and the total area expanded by 0.15 km². From August 1996 to July 1997, the eastern terminus advanced 40 ± 21 m, the western terminus advanced 134 ± 21 m, and the total area expanded 0.20 ± 0.02 km². The Landsat image from September 1997 shows that the glacier had begun to retreat.

4.3. Glacier Surging during 2014–2016

According to Landsat images (Figure 4), we found that Kyagar Glacier showed signs of advancing (38 m) on 28 April 2014, and then advanced another 97 ± 21 m by September 2014. From September 2014 to April 2015, the glacier advanced 278 ± 21 m, indicating that the advance was faster in winter. Following this, the advance was slower, proceeding only 25 ± 21 m until July 2015. From July to October 2015, there was little change at the terminus. The following winter, however, the glacier advanced 43 ± 21 m by March 2016. According to a Landsat image from September 2016, the west side of the glacier terminus advanced by 30 ± 21 m, while the east side of the terminus also advanced by 40 ± 21 m after March

2016. There was no sign of glacier advancement according to Landsat images taken after September 2016.

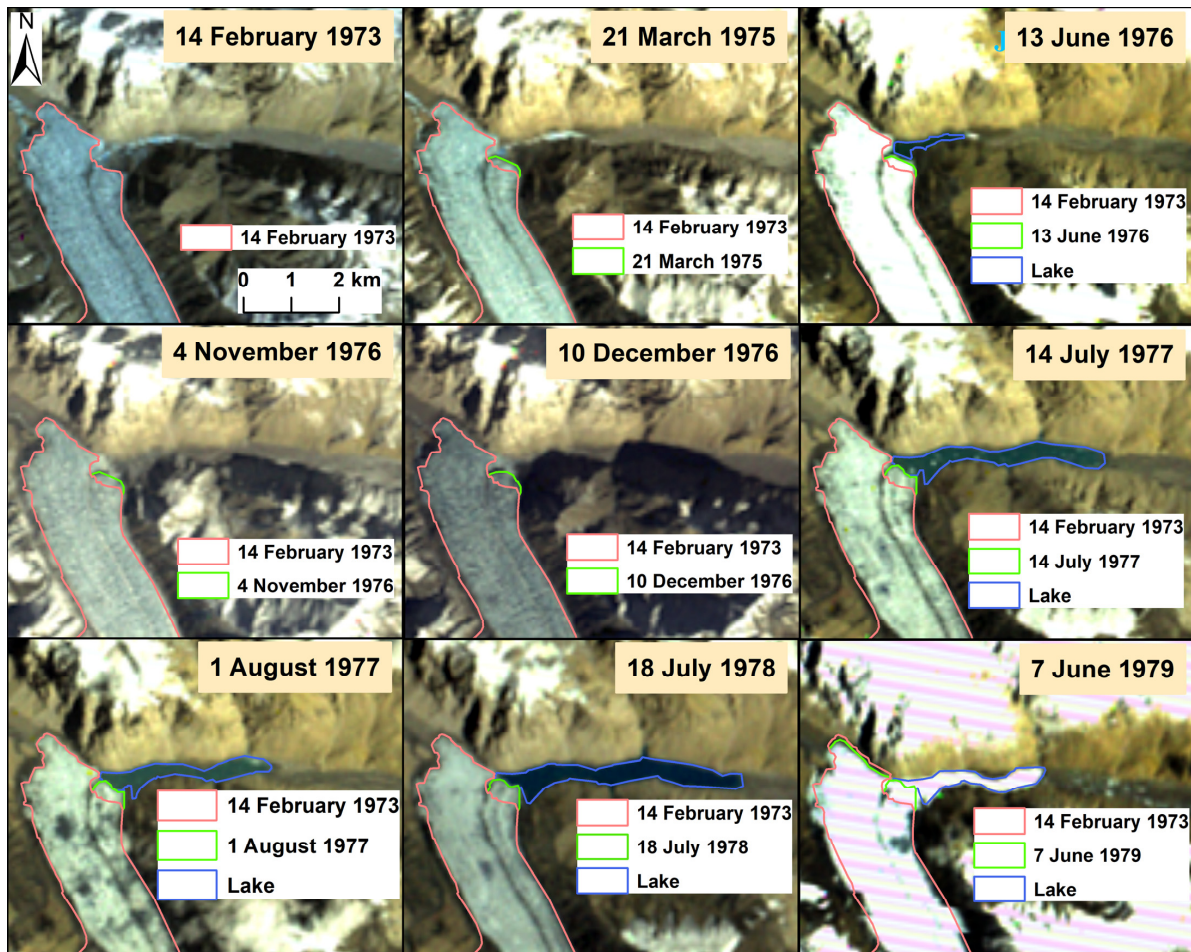


Figure 2. Glacier boundary and glacial lake boundary in different periods from 1975 to 1978.

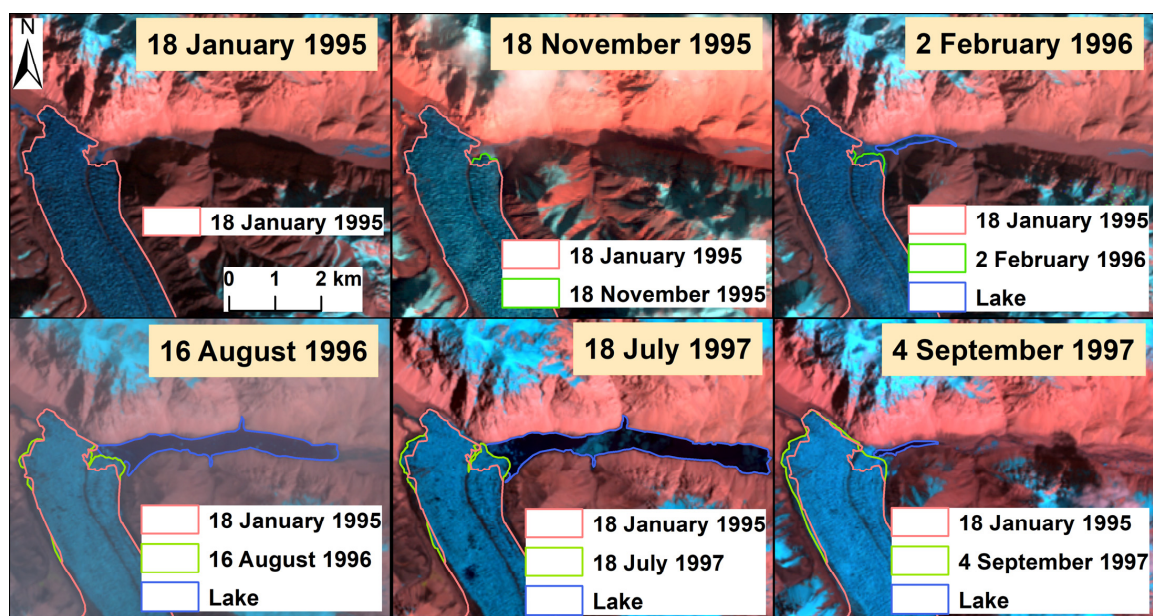


Figure 3. Glacier and glacial lake boundaries in different periods from 1995 to 1997.

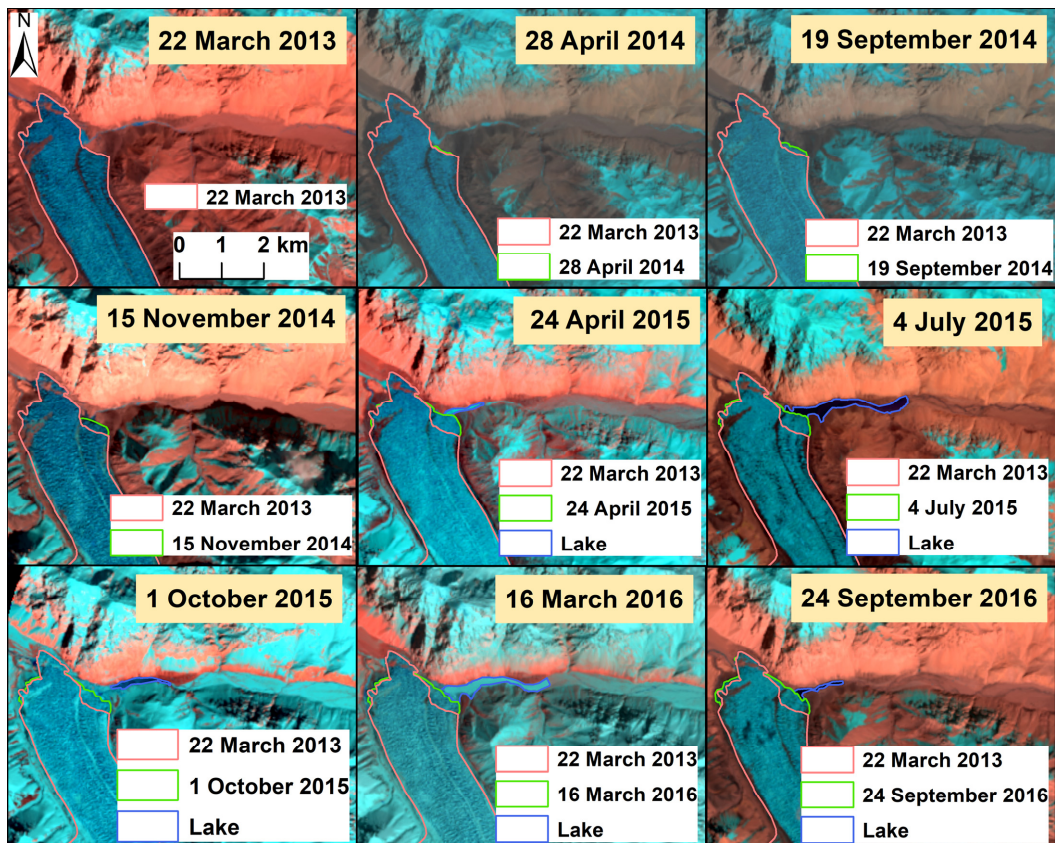


Figure 4. Glacier and glacial lake boundaries in different periods from 2013 to 2016.

In Summary, the Kyagar Glacier has undergone three surges since 1975, with an active period of 2–3 years and a maximum advance of 521 ± 21 m. There was a rapid advance within 10 months of the surge start, which was followed by a slow advance. Another rapid advance occurred within 20–28 months of the first surge (Figure 5).

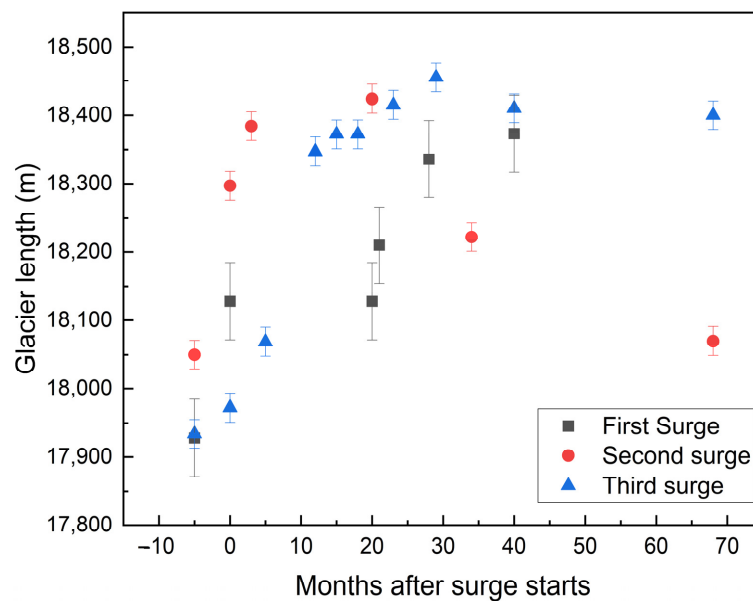


Figure 5. The change in the length of the glacier over a period of time after the beginning of the surge. A negative abscissa means before the surge. The error bar represents uncertainty in the length of the glacier.

4.4. Glacier Velocity Changes

According to the time series of glacier velocities derived from ITS_LIVE during 1989–2018 (Figures 6 and 7), it can be seen that the average maximum velocity of Kyagar Glacier from 1989 to 1994 was $185 \pm 3 \text{ m a}^{-1}$. The glacier velocity suddenly increased in 1995 ($318.2 \pm 3 \text{ m a}^{-1}$) and peaked at $452 \pm 7 \text{ m a}^{-1}$ in 1996. Then, the glacier slowed in 1997 ($294.2 \pm 4 \text{ m a}^{-1}$) and returned to its normal velocity in 1998 ($194.5 \pm 4 \text{ m a}^{-1}$). Therefore, there was a surge event in 1995–1997.

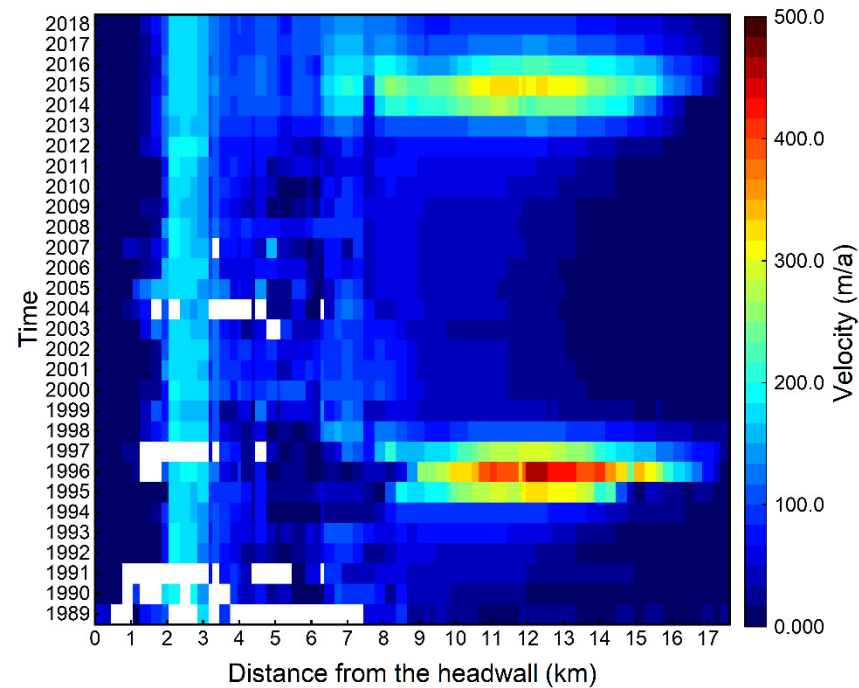


Figure 6. Spatial and temporal distributions in glacier velocity along the longitudinal profile in Figure 1 during 1989–2018 (Data source: ITS_LIVE).

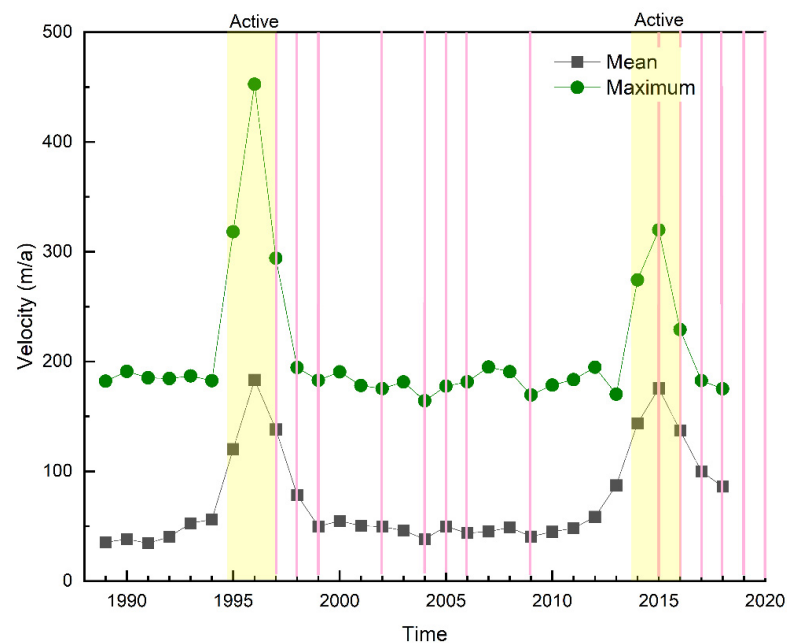


Figure 7. Curves of mean and maximum glacier velocities with time. Pink vertical lines represent GLOF events. Historical GLOF records were from Round et al. [30] and our study. We determine GLOF events based on the disappearance of glacial lakes in remote sensing images.

From 1998 to 2013, the average maximum velocity of the glacier was $182 \pm 3 \text{ m a}^{-1}$. It began to accelerate sharply again in 2014 ($274.3 \pm 1 \text{ m a}^{-1}$), peaked at $319 \pm 1 \text{ m a}^{-1}$ in 2015, and began to slow down in 2016 ($229.0 \pm 1 \text{ m a}^{-1}$) before returning to its normal velocity in 2017 ($182.6 \pm 1 \text{ m a}^{-1}$). Therefore, there was a surge event in 2014–2016.

Although there are no data on changes in glacier velocity from 1973 to 1978, the glacier advanced 208 m in less than one year from November 1976 to July 1977 (Figure 2). We speculate that the velocity peaked in 1976–1977 at $>200 \text{ m a}^{-1}$. Therefore, there was a surge event in 1973–1978.

The glacier velocity continued to decrease from 1998 to 2004 (Figure 7), was relatively stable from 2005 to 2009, and increased slightly from 2010 to 2013. Therefore, the period from 1998 to 2009 was the quiescent phase of the last surge, and the period from 2010 to 2013 was a buildup phase before the next surge. The glacier also showed a slightly increasing trend from 1991 to 1994, which may be the buildup phase before the 1995–1997 surge.

According to Sentinel-1 data from October 2014 to April 2021 (Figure 8), the glacier's monthly velocity was significantly higher from October 2014 to July 2015 than in other months. In fact, the glacier began to be active on 28 April 2014 (Figure 4 and Table 2). From October 2014 to February 2015, the glacier velocity reached its peak ($2 \pm 0.08 \text{ m d}^{-1}$). However, the glacier slowed sharply in August 2015 to a maximum velocity of only $0.7 \pm 0.08 \text{ m d}^{-1}$. From January to May 2016, the maximum velocity was only $0.5\text{--}0.6 \text{ m d}^{-1}$. From June to July 2016, the maximum velocity was $0.8 \pm 0.08 \text{ m d}^{-1}$, which then decreased significantly in August (maximum velocity = 0.6 m d^{-1}). From 2017 to 2019, there were seasonal differences in glacier velocity, being generally faster in June and July (summer). The glacier velocity showed an overall downward trend after 2016. After 2020, the seasonal differences were less significant, and the maximum velocity was 0.2 m d^{-1} . We also found that the water storage process before the GLOF resulted in an increase in the glacier velocity, and the glacier velocity decreased rapidly after the GLOF. As the height of the ice dam continued to drop, the water storage was getting smaller and smaller, and the glacier velocity was also decreasing year by year. If the ice dam continues to descend and disappears, the GLOF will not occur until the next surge.

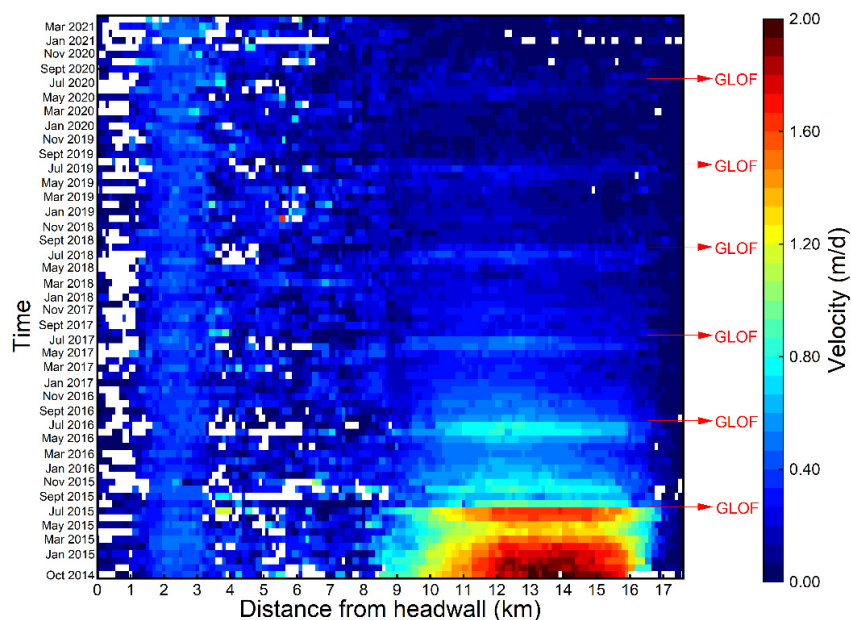


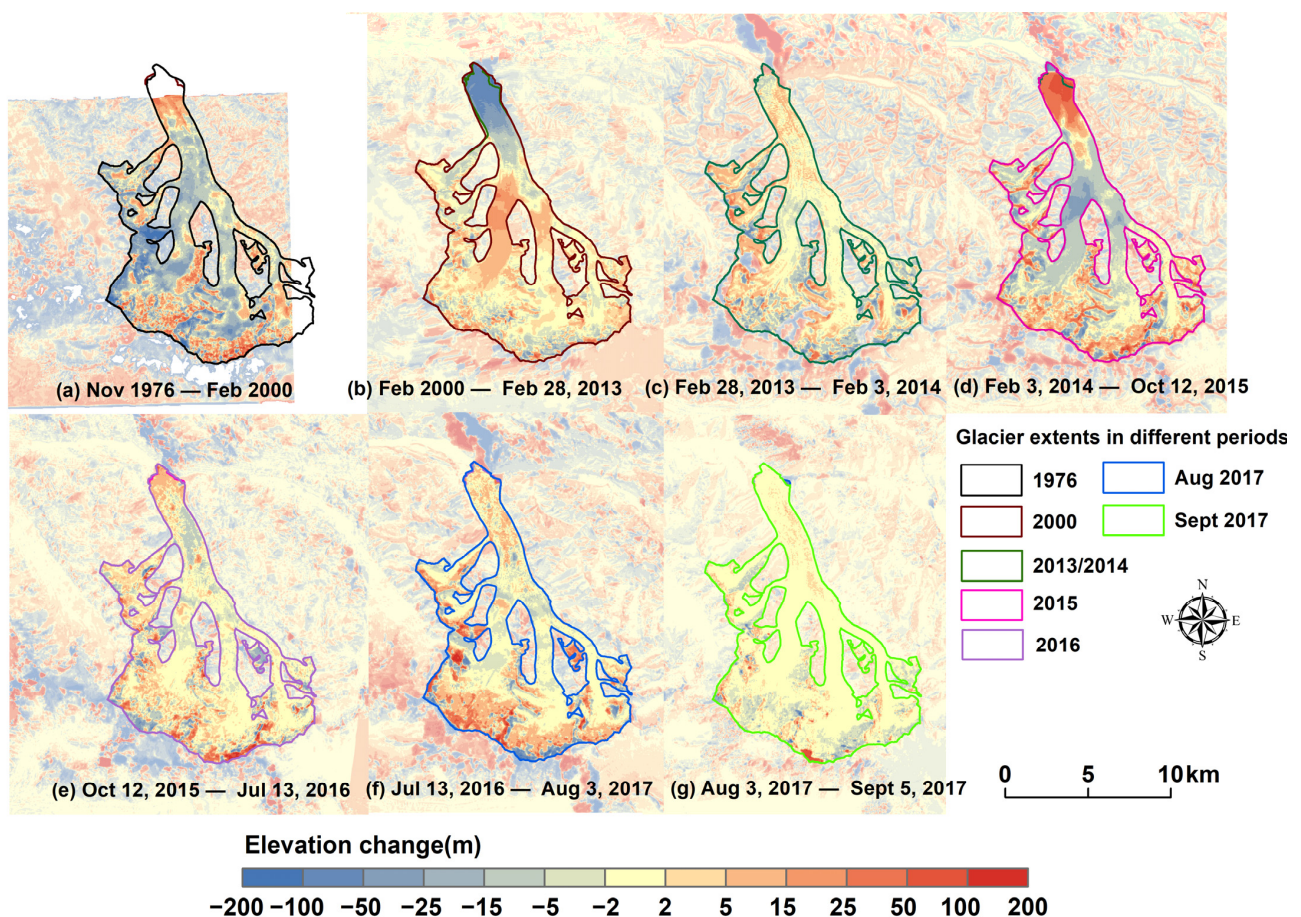
Figure 8. Spatial and temporal distributions in glacier velocity along the longitudinal profile in Figure 1 during 2014–2021.

Table 2. Maximum velocity of glacier flow before and after the surge in 2014–2016.

Period	Maximum Velocity (m d^{-1})
Before 28 April 2014	0.5 ± 0.08
From 28 April to 30 May 2014	1 ± 0.08
From October 2014 to February 2015	2 ± 0.08
From March to May 2015	1.5 ± 0.08
From June to July 2015	1.7 ± 0.08
August 2015	0.7 ± 0.08
From January to May 2016	0.5 ± 0.08
From June to July 2016	0.8 ± 0.08
August 2016	0.6 ± 0.08

4.5. Glacier Elevation Changes during 1976–2017

Based on TOPO DEM (1976), SRTM (2000), and TerraSAR-X/TanDEM-X (2013–2017) data, glacier elevation changes in seven time periods were obtained (Figures 9 and 10). Despite a lack of data on elevation changes in the glacier terminus from 1976 to 2000, it can still be seen that there was a significant thickening of the terminus. The glacier thickness increased by 14 ± 1.1 m (on average) between 2 km and 4 km of the terminus and decreased by 12 ± 1.1 m (on average) between 4 km and 15 km of the terminus during 1976–2000.

**Figure 9.** Glacier elevation changes in different periods.

The elevation changes from 2000 to 2013 show that the glacier terminus exhibited a significant thinning trend (average thinning = 56 ± 0.4 m). Meanwhile, the elevation above the west branch confluence increased by 17 ± 0.4 m, while that above the east branch confluence increased by 9 ± 0.4 m at most. This elevation variation is typical of a glacier's

quiescent phase, which features thinning of the terminal's elevation and buildup of ice above the west branch confluence.

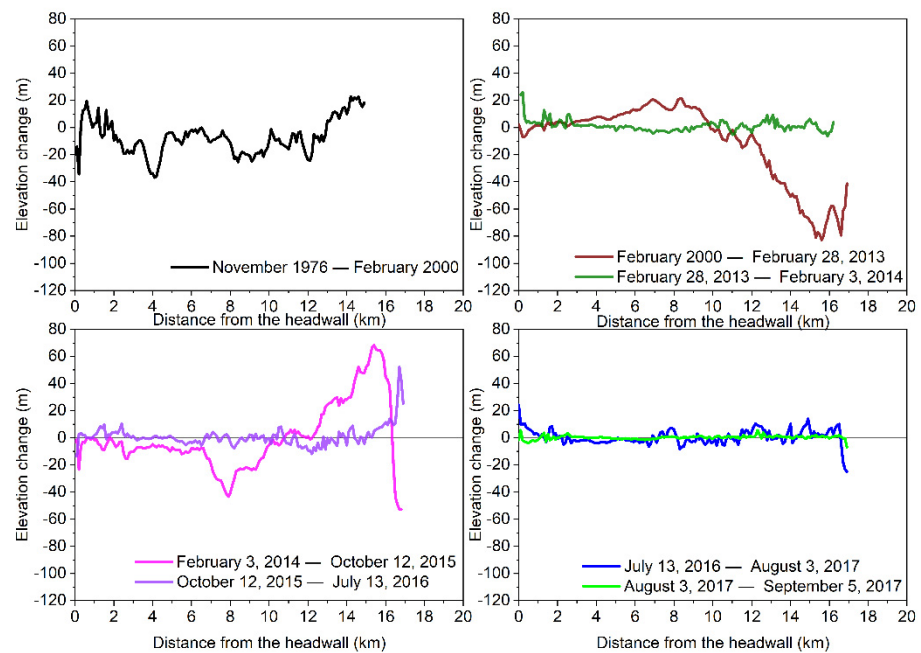


Figure 10. Glacier elevation change profiles in different periods (the longitudinal profile in Figure 1).

There was a slight elevation change of the glacier surface from 2013 to 2014, a slight thickening at the terminus, and a slight thinning in the reservoir zone of the western branch at the upper part of the confluence. These indicate that ice had begun to transfer from the reservoir zone to the terminus.

From 2014 to 2015, the glacier terminus thickened sharply, the reservoir zone (>6 km from the terminus) thinned by 12 ± 0.2 m, and the terminal receiving zone (0.5–6 km from the terminus) thickened by 28 ± 0.2 m, which are typical characteristics of surging. From 2015 to 2016, the glacier thickness increased by 28 m at 0–0.5 km from the terminus, indicating that the surge front moved to the terminus and led to its advance, especially of the eastern terminus. After July 2016, the elevation change of the glacier was relatively weak and the terminus began to show signs of thinning.

4.6. Glacial Lake Formation

During the first surge period (1975–1978), a terminal glacial lake with an area of 0.23 km^2 could be seen in the 13 June 1976 image (Figure 2). However, this glacial lake could not be seen in the image of November 1976, indicating that there was a glacial lake burst during the period. The Landsat image of 14 July 1977 shows that the new terminal glacial lake reached 1.52 km^2 in area and burst on 16 July 1977 [30]. The image of 1 August 1977, shows that a new glacial lake had formed (1.07 km^2), expanding to 1.92 km^2 on 18 July 1978, and bursting on 6 September 1978 (Table 3), with the surge probably stopping at the same time [30].

During the second surge period (1995–1997), the terminal glacial lake area reached its maximum area of 2.78 km^2 in July 1997 (Figure 3), then burst on 3 August 1997 [30]. The Landsat image of September 1997 shows that a new terminal glacial lake had formed. Therefore, the glacier surge probably ended in August 1997 when the glacial lake burst.

During the third surge period (2014–2016), a terminal glacial lake had formed that covered an area of 0.08 km^2 by April 2015 (Figure 4). The lake area reached an area of 0.55 km^2 on 4 July 2015 and burst on 27 July [30]. Landsat images taken on 1 October 2015, show that another terminal glacial lake had formed, reaching 0.48 km^2 in area by March 2016, and bursting on 17 July 2016 [30]. Considering the 2016 glacier velocities, we suggest that the end time of the glacier surge may have been July 2016, which also corresponds to the timing of the GLOF event.

Table 3. Glacial lake area and volume change.

Time	Lake Area (m ²)	Lake Volume (mio. m ³)
13 June 1976	0.23	6.13
14 July 1977	1.52	58.93
1 August 1977	1.07	42.17
18 July 1978	1.92	114.10
7 June 1979	0.91	35.81
2 February 1996	0.22	5.56
16 August 1996	2.01	131.03
18 July 1997	2.78	214.83
4 September 1997	0.13	0.99
24 April 2015	0.08	0.63
4 July 2015	0.55	25.95
1 October 2015	0.15	1.90
16 March 2016	0.48	15.26
24 September 2016	0.10	0.64

There were 29 GLOF events from 1959 to 2020 (Figure 11). In the first surge cycle (1972–1990), seven GLOF events occurred. In the second surge cycle (1991–2009), there were eight GLOFs. The last GLOF event of the quiescent phase was in 2009. In the third surge cycle (since 2010), there have been six GLOFs, including two in the active phase. This quiescent phase is not over yet and there may be more GLOFs in the future. There were eight GLOF events from 1959 to 1971, and 1959 may have been an active period. The final GLOF event of the quiescent phase was in 1971. In addition, analysis of changes in temperature and precipitation derived from ERA5 data found that GLOFs were not strongly correlated with these factors.

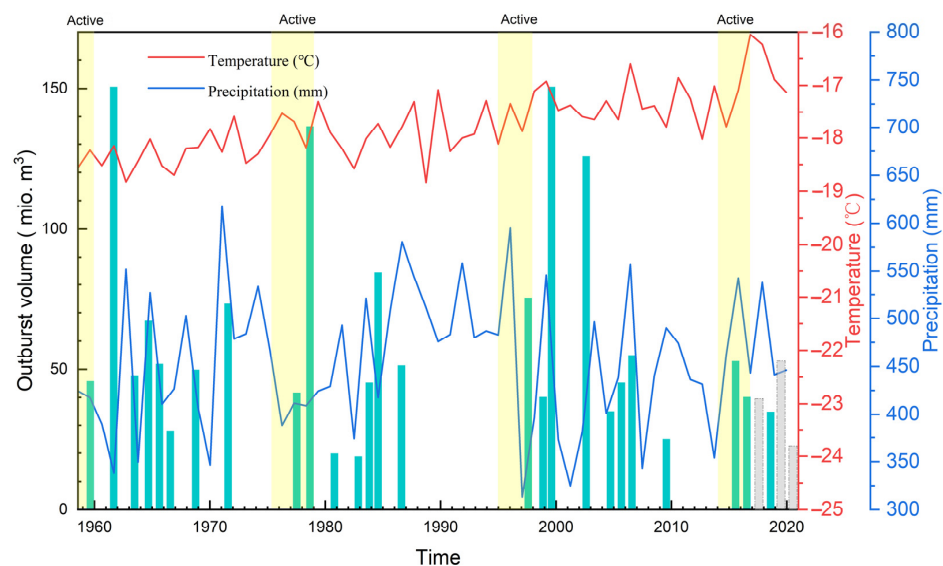


Figure 11. Glacial lake outburst volumes (columns) and annual temperature and precipitation times series from 1959 to 2020. The volumes were derived from (1) 1959–2016 = Round et al. [30], (2) 2018 = Zhang et al. [45], and (3) 2017, 2019, and 2020 = estimates of lake areas in satellite images according to the method of Round et al. [30]. Temperature and precipitation were derived from ERA5 data.

5. Discussion

5.1. Methodological Aspects

The original resolution of Landsat MSS images was 79 m, so the uncertainty in glacier length changes was 56 m and that of area changes was 0.06 km². During the first surging period, the east side of the glacier advanced 445 m and its area expanded by 0.13 km², both

of which are greater than the uncertainties. From November 1976 to July 1977, the glacier advanced by 208 m. Even after subtracting the uncertainty of 56 m, the glacier advanced by more than 100 m a^{-1} , which can be confirmed as a surge [46].

Landsat TM and ITS_LIVE data were used for the second surging judgment. The resolution of Landsat TM was 30 m, the uncertainty in glacier length change was 21 m, and the uncertainty in area change was 0.09 km^2 . During the second surging period, the east side of the glacier advanced 374 m, the west side advanced 209 m, and the total area expanded by 0.59 km^2 , all of which are greater than the uncertainty. Moreover, according to the ITS_LIVE glacier velocity error results, the maximum error in glacier velocity during 1995–1997 was 6.8 m a^{-1} , which is far lower than the peak velocity during this surging period (452 m a^{-1}).

The third surging period was determined using Landsat OLI, ITS_LIVE, Sentinel-1 glacier velocity, and TerraSAR-X/TanDEM-X data. The maximum resolution of Landsat OLI was 15 m, the uncertainty in glacier length change was 11 m, and the uncertainty in area change was 0.03 km^2 . During the third surging period, the east side of the glacier advanced 481 m, the west side advanced 30 m, and the total area expanded by 0.42 km^2 , which are all greater than the uncertainty. According to ITS_LIVE glacier velocity data error results [41], the maximum error in glacier velocity in 1995–1997 was 0.4 m a^{-1} , which is far lower than the peak velocity (319 m a^{-1}) during this surging period. The uncertainty in Sentinel-1 glacier velocity data is 0.08 m^{-1} [47], which is also less than the peak monthly mean velocity (2 m^{-1}). The uncertainty in glacier elevation changes during 2013–2017 derived from TerraSAR-X/TanDEM-X was 0.2 m, which is far lower than the glacier elevation change during this surge event ($>60 \text{ m}$).

In this study, we also used SRTM (C-band) data as auxiliary data to analyze glacier elevation changes during 1976–2000 and 2000–2013. The SRTM can penetrate snow and ice to a certain extent [48]. Round et al. [30] suggested that the C-band penetration in Kyagar Glacier was $<4 \text{ m}$, while penetration of the glacier tongue was 1–2 m. The terminal thickening of Kyagar Glacier from 1976 to 2000 is underestimated due to this penetration, so the terminal thickening is more certain. The glacier terminal thinning from 2000 to 2013 is also underestimated, and it is indisputable that there was terminal thinning during this period.

5.2. Glaciological Aspects

Round et al. [30] suggested that the surging of Kyagar Glacier is hydrologically controlled. The most important basis for this judgment is that the surging stopped after the outburst of the terminal glacial lake. They believe that when the terminal GLOF occurred in July 2015, the velocity of the glacier plunged and the surging stopped. Our results (Figures 6 and 8) also show that there was a sharp drop in velocity in July 2015. However, we found that the glacier terminus was still advancing in 2016 (Figure 4). Combined with the fact that the glacier velocity was still higher in 2016 (Figure 6) and that there was a sharp decline after July 2016 when the terminal GLOF occurred, we suggest that the glacier surging stopped after the GLOF in July 2016. Bhabri et al. [14] also suggested that the surging of Kyagar Glacier ended in 2016. Therefore, we extended the active phase of this surge to 2–3 years, which is consistent with the previous two surges.

The glacier surge causes a large amount of material to transfer from upstream to downstream, forming an ice dam and creating conditions for GLOF. At the end of the surge, the drainage channel at the base of the glacier becomes effective and the water inside the glacier is released [30]. The raising of ice dam due to the surge often leads to the outburst of the glacial lake, and the surge usually ends at the end of GLOF. However, after a period of time, the glacial lake still undergoes outburst events, usually 7–8 times. Such GLOFs are not directly related to temperature and precipitation (Figure 11), although an increase in temperature will accelerate glacier melting. During a surge, ice from the high-altitude reservoir zone is transferred to the downstream low-altitude receiving zone, and low-altitude ice can melt more as the temperature increases. Glacial meltwater also provides water for the formation of GLOF. The rate of decrease in the elevation of the ice

dam was $>5 \text{ m a}^{-1}$ during the quiescent phase, which is consistent with Haemmig et al. [28] and Bhambri et al. [21]. This cycle of GLOF ends when the dam is low enough to block the river any longer. This is why there was no GLOF between 1972–1976, 1987–1996, and 2010–2014.

The time intervals of the three surges were similar; they occurred every 19–20 years, with an active phase of 3–4 years and a quiescent phase of 16–17 years. Therefore, we speculate that there may have been a surge in 1955–1959 with an initiation time of 1955–1957 and a termination time of 1958–1959. Glacier surges in the Alaska-Yukon, Pamir, and Iceland regions have similar cycles to the Kyagar Glacier, with most of the cycles being around 20–40 years in duration with the active phase being around 1–3 years [49–51]. The cycle length of a surging glacier is generally considered to be related to the accumulation (snowfall) rate of mass in the reservoir zone. That is, a surging glacier with a rapid accumulation of mass in the reservoir zone has a short cycle, while one with slow accumulation has a long cycle [52]. The surging period of Svalbard glaciers is 50–500 years with active phases lasting 4–10 years [53]. The snowfall rate in Svalbard is relatively low, and the rate of accumulation of mass in the reservoir zone is slow, so the surging period is relatively long. The cycle also changes with climate change. The Eyjabakkajökull Glacier in Iceland had a cycle of 21–23 years in the 17th and 18th centuries and cycles of 34–38 years in the modern era [54]. In the context of climate change, if there is not enough mass accumulation to recharge the reservoir zone, a surging glacier may gradually become non-surging. Dowdeswell et al. [55] found that there were 18 surging glaciers in Svalbard in 1936–1938 but only five in 1990 and suggested that this trend reflects a continuous negative mass balance at the end of the 20th century. Although this conclusion has yet to be tested, some of the smaller glaciers that have surged before are showing strong negative mass balances and seem to be losing their ability to surge. In the Austrian Alps, for example, there were four surging glaciers during the Little Ice Age but now there are none [56].

5.3. Comparison with Other Surge-Type Glaciers in the Karakoram

The Karakoram region has a concentration of at least 220 surge-type glaciers (including tributaries), with 38 glaciers having been observed to surge twice or more [14]. Paul [19] added 16 glaciers that have surged twice or more. Based on the previous literature, we established 28 glacier surge cycles, among which the shortest is 5–8 years and the longest is more than 60 years (Table 4). Although two surges have been recorded for some glaciers, the cycles are too long (e.g., >100 years). Due to the limited availability of remote sensing data, there is insufficient evidence to prove whether there was a surge in the interval. Of course, it is possible that some surge-type glacier cycles may be longer than 100 years. Therefore, the periodicity of surge-type glaciers in the Karakoram is heterogeneous, which may be related to the thermal properties of the ice (cold / polythermal) and the environment. The surge cycles of the Hasanabad, Staghar, and Khurdopin glaciers are similar to that of the Kyagar Glacier. Among them, Khurdopin Glacier had six surging periods from 1880 to 2020, with active phases of 3–4 years and 19–20-year cycles [24], which is similar to Kyagar. Interestingly, the Khurdopin Glacier surging also led to repeated GLOFs.

Table 4. Characteristics of Karakoram surging glaciers observed to have surged at least twice.

GLIMS ID	Glacier Name	Glacier Area (km ²)	Active Phase (year)	Surge Cycle (year)	Whether It Causes GLOF by Surging (Number of GLOFs Caused by a Surge Cycle)	References
G077158E35562N	Kyagar	97.10	1975–1978 (3) 1995–1997 (2) 2014–2016 (2)	19–20	Yes (7–8)	This study
G075308E36242N	Yazghil	133.75	1997–1998 (2) 2005–2006 (2) 2010–2011 (2) 2018–2019 (2)	5–8	Yes	[14]

Table 4. Cont.

GLIMS ID	Glacier Name	Glacier Area (km ²)	Active Phase (year)	Surge Cycle (year)	Whether It Causes GLOF by Surging (Number of GLOFs Caused by a Surge Cycle)	References
G077294E35212N		5.51	1976–1978 (3) 1991–1994 (4) 2006–2010 (5)	15	No	[14]
G076960E35666N	First Singhi	8.49	1990–1996 (7) 2008–2011 (4)	18	No	[14]
G076900E35638N	Staghar	76.13	1989–1991 (3) 2009–2011 (3)	20	Yes	[14]
G074619E36437N	Hassanabad	45.71	1995–1997 (3) 2014–2016 (3)	19	Yes	[14]
G077662E35097N	Kichik Kumdun	66.24	1902–1903 (2) 1935–1936 (2) 1970–1972 (3) 1998–2000 (3)	28–35	Yes	[14]
G075680E35803N	Tonga	11.33	1990–1994 (4) 2014–2016 (2)	24	No	[14]
G074581E36501N	Batura	311.65	1990–1995 (5) 2005–2010 (5) 2013–2018 (5)	8–15	Yes	[14]
G074990E36246N	Gharsa	78.00	1995–1997 (2) 2001–2003 (2) 2015–2015 (1)	6–14	No	[14]
G075218E35874N	West Marpoh	295.32	1995–1998 (3) 2005–2006 (1) 2013–2015 (2)	8–10	No	[14]
G075438E36192N	Khurdopin	203.34	1977–1979 (3) 1998–2002 (4) 2016–2020 (4)	19–20	Yes (6)	[14,24]
G075653E36149N	Virjerab	167.43	2004–2007 (4) 2018–?	14	Yes	[14]
G076036E35822N	1st Feriole	12.92	1953–1973 (20) 1998–2017 (20)	45	No	[19]
G076049E35853N	Shingchukpi	14.51	1950–1960 (10) 1995–2006 (10)	45	No	[19]
G075959E35848N (Chiring)		334.69	1955–1960 (5) 1992–1995 (3)	35–40	No	[19]
G075959E35848N (Drenmang)		334.69	1964–1967 (3) 2005–2007 (2)	35–40	No	[19]
G076298E35850N (Sarmo Laggo)		199.17	1950–1955 (5) 1993–1998 (5)	40	No	[19]
G076298E35850N (NN7)		199.17	1953–1963 (10) 1998–2009 (9)	45	No	[19]
G076298E35850N (NN10)		199.17	1945–1950 (5) 1993–2001 (8)	50	No	[19]
G076261E35935N		3.85	1954–1961 (7) 1980–1987 (7) 2002–2010 (8)	20–25	No	[19]
G076406E35964N		3.35	1980–1990 (10) 2000–2010 (10)	20	No	[19]
G076267E35990N		7.16	1945–1960 (15) 1995–2010 (15)	50	No	[19]

Table 4. Cont.

GLIMS ID	Glacier Name	Glacier Area (km ²)	Active Phase (year)	Surge Cycle (year)	Whether It Causes GLOF by Surging (Number of GLOFs Caused by a Surge Cycle)	References
G076247E36088N		11.54	1980–1995 (15) 2005–2018 (13)	35	No	[19]
G076225E36119N (North Crown)		57.58	1950–1955 (5) 2008–2013 (5)	60	No	[19]
G076225E36119N (NN30)		57.58	1953–1958 (5) 1981–1986 (5) 2008–2015 (7)	27	No	[19]
G076417E36281N	Tatulu Guo	29.91	1940–1955 (15) 2002–2017 (15)	60	No	[19]
G075997E36267N	Saxinitulu	39.51	1955–1960 (15) 2009–2015 (15)	55	No	[19]

The mechanism of Karakoram glacier surging is relatively complex and may be controlled by three types of factors—thermal, hydrological, and geomorphological—to different degrees in different glaciers [16,57,58]. Round et al. [30] determined that the surging of Kyagar Glacier is hydrologically controlled. Its peak surge velocity (2.5 m d⁻¹) is less than those of the Khurdopin (14.2 m d⁻¹), Hispar (14 m d⁻¹), and Shispare Glaciers (18 m d⁻¹), which have been identified as hydrologically controlled glaciers [17,59,60]. Paul et al. [61] indicated that a transition from one mechanism to another may occur during a surge. Therefore, the Karakoram glacier surge mechanism is complex, and complete cycle monitoring is helpful to further understand the glacier surge mechanism. We suggest that future studies strengthen the monitoring of repeated glacier surges. The timing of the formation of the ice dam lake and the GLOF can be estimated for some surging glaciers, providing time for residents and authorities to take preventive measures to limit downstream damage.

6. Conclusions

Landsat, topographic map, SRTM, TerraSAR-X/TanDEM-X, ITS_LIVE, and Sentinel-1 glacier velocity data were used to identify three surge events since the 1970s. The three surges occurred with a similar pattern, being a 19–20-year cycle with a 3–4-year active phase and a 16–17-year quiescent phase. The active phases of these three cycles occurred in 1975–1978, 1995–1997, and 2014–2016, respectively. In a recent surge (2014–2016), the maximum velocity was 2 m d⁻¹ in the active phase. The glacier terminal thickened sharply while the reservoir zone thinned by 12 m and the terminal receiving zone thickened by 28 m. The glacier may have entered a quiescent phase after July 2016 when a GLOF event occurred. Each surge would cause 7–8 GLOF events. The glacier surge causes a large amount of material to transfer from upstream to downstream, forming an ice dam and creating conditions for a GLOF event. In the repeated process of GLOFs, the ice dam elevation continuously decreased. Finally, the ice dam disappeared, and the GLOF no longer continued before the next glacier surging. The results of this study help to better understand glacial surge cycles, which will be useful for further insights into the responsible surge mechanism.

Author Contributions: Conceptualization, Z.Z.; methodology, Z.Z.; software, Z.Z., J.Z. and Z.J.; validation, Z.Z.; formal analysis, Z.Z.; investigation, Z.Z.; resources, Z.Z., Z.J. and Q.Z.; data curation, Z.Z.; writing—original draft preparation, Z.Z.; writing—review and editing, Z.Z. and S.L.; visualization, Z.Z., Y.X. and J.Z. and H.S.; supervision, S.L.; project administration, Z.Z.; funding acquisition, Z.Z. All authors have read and agreed to the published version of the manuscript.

Funding: This research was funded by the Major Project on Natural Science Foundation of Universities in Anhui Province (Grant No. 2022AH040111), the National Natural Science Foundation of China (Grant Nos. 42071085 and 41701087) and the Natural Science Foundation of Hunan Province (Grant No. 2022JJ30243).

Institutional Review Board Statement: Not applicable.

Informed Consent Statement: Not applicable.

Data Availability Statement: The data presented in this study are available on request from the author.

Acknowledgments: We thank the USGS and NASA for the Landsat, SRTM, and ITS_LIVE data; the German Aerospace Centre for access to TerraSAR-X/TanDEM-X data (proposal ID: NTL_BIST3395); ECMWF for the ERA5 data. We also thank Friedl et al. [25] for access to Sentinel-1 glacier velocities.

Conflicts of Interest: The authors declare no conflict of interest.

References

1. Jiskoot, H. Glacier Surging. In *Encyclopedia of Snow, Ice and Glaciers*; Singh, V.P., Singh, P., Haritashya, U.K., Eds.; Springer: Dordrecht, The Netherlands, 2011; pp. 415–428.
2. Dolgoushin, L.D.; Osipova, G.B. *Glacier Surges and the Problem of Their Forecasting*; IAHS Publication: Wallingford, UK, 1975; pp. 292–304.
3. Cuffey, K.M.; Paterson, W.S.B. *The Physics of Glaciers, Glaciology*, 4th ed.; Butterworth-Heinemann/Elsevier: Burlington, NJ, USA, 2010.
4. Wilson, R.; Harrison, S.; Reynolds, J.; Hubbard, A.; Glasser, N.F.; Wünderlich, O.; Iribarren Anaconda, P.; Mao, L.; Shannon, S. The 2015 Chileno Valley glacial lake outburst flood, Patagonia. *Geomorphology* **2019**, *332*, 51–65. [[CrossRef](#)]
5. Haga, O.N.; McNabb, R.; Nuth, C.; Altena, B.; Schellenberger, T.; Kaab, A. From high friction zone to frontal collapse: Dynamics of an ongoing tidewater glacier surge, Negribreen, Svalbard. *J. Glaciol.* **2020**, *66*, 742–754. [[CrossRef](#)]
6. Paul, F. Repeat Glacier Collapses and Surges in the Amney Machen Mountain Range, Tibet, Possibly Triggered by a Developing Rock-Slope Instability. *Remote Sens.* **2019**, *11*, 708. [[CrossRef](#)]
7. Sevestre, H.; Benn, D.I. Climatic and geometric controls on the global distribution of surge-type glaciers: Implications for a unifying model of surging. *J. Glaciol.* **2015**, *61*, 646–662. [[CrossRef](#)]
8. Falaschi, D.; Bolch, T.; Lenzano, M.G.; Tadono, T.; Lo Vecchio, A.; Lenzano, L. New evidence of glacier surges in the Central Andes of Argentina and Chile. *Prog. Phys. Geogr. Earth Environ.* **2018**, *42*, 792–825. [[CrossRef](#)]
9. Miles, E.; McCarthy, M.; Dehecq, A.; Kneib, M.; Fugger, S.; Pellicciotti, F. Health and sustainability of glaciers in High Mountain Asia. *Nat. Commun.* **2021**, *12*, 2868. [[CrossRef](#)]
10. Brun, F.; Berthier, E.; Wagnon, P.; Kaab, A.; Treichler, D. A spatially resolved estimate of High Mountain Asia glacier mass balances, 2000–2016. *Nat. Geosci.* **2017**, *10*, 668–673. [[CrossRef](#)] [[PubMed](#)]
11. Bolch, T.; Pieczonka, T.; Mukherjee, K.; Shea, J. Brief communication: Glaciers in the Hunza catchment (Karakoram) have been nearly in balance since the 1970s. *Cryosphere* **2017**, *11*, 531–539. [[CrossRef](#)]
12. Lin, H.; Li, G.; Cuo, L.; Hooper, A.; Ye, Q. A decreasing glacier mass balance gradient from the edge of the Upper Tarim Basin to the Karakoram during 2000–2014. *Sci. Rep.* **2017**, *7*, 6712. [[CrossRef](#)]
13. Hewitt, K. The Karakoram anomaly? Glacier expansion and the ‘elevation effect,’ Karakoram Himalaya. *Mt. Res. Dev.* **2005**, *25*, 332–340. [[CrossRef](#)]
14. Bhambri, R.; Hewitt, K.; Kawishwar, P.; Pratap, B. Surge-type and surge-modified glaciers in the Karakoram. *Sci. Rep.* **2017**, *7*, 15391. [[CrossRef](#)] [[PubMed](#)]
15. Copland, L.; Sylvestre, T.; Bishop, M.P.; Shroder, J.F.; Seong, Y.B.; Owen, L.A.; Bush, A.; Kamp, U. Expanded and Recently Increased Glacier Surging in the Karakoram. *Arct. Antarct. Alp. Res.* **2011**, *43*, 503–516. [[CrossRef](#)]
16. Quincey, D.J.; Glasser, N.F.; Cook, S.J.; Luckman, A. Heterogeneity in Karakoram glacier surges. *J. Geophys. Res. Earth Surf.* **2015**, *120*, 1288–1300. [[CrossRef](#)]
17. Paul, F.; Strozzi, T.; Schellenberger, T.; Käab, A. The 2015 Surge of Hispar Glacier in the Karakoram. *Remote Sens.* **2017**, *9*, 888. [[CrossRef](#)]
18. Singh, R.M.; Govil, H.; Shahi, A.P.; Bhambri, R. Characterizing the glacier surge dynamics in Yarkand basin, Karakoram using remote sensing. *Quat. Int.* **2021**, *575–576*, 190–203. [[CrossRef](#)]
19. Paul, F. A 60-year chronology of glacier surges in the central Karakoram from the analysis of satellite image time-series. *Geomorphology* **2020**, *352*, 106993. [[CrossRef](#)]
20. Goerlich, F.; Bolch, T.; Paul, F. More dynamic than expected: An updated survey of surging glaciers in the Pamir. *Earth Syst. Sci. Data* **2020**, *12*, 3161–3176. [[CrossRef](#)]
21. Bhambri, R.; Hewitt, K.; Haritashya, U.K.; Chand, P.; Kumar, A.; Verma, A.; Tiwari, S.K.; Rai, S.K. Characteristics of surge-type tributary glaciers, Karakoram. *Geomorphology* **2022**, *403*, 108161. [[CrossRef](#)]
22. Zhu, Q.; Ke, C.-Q.; Li, H. Monitoring glacier surges in the Kongur Tagh area of the Tibetan Plateau using Sentinel-1 SAR data. *Geomorphology* **2021**, *390*, 107869. [[CrossRef](#)]
23. King, O.; Bhattacharya, A.; Bolch, T. The presence and influence of glacier surging around the Geladandong ice caps, North East Tibetan Plateau. *Adv. Clim. Change Res.* **2021**, *12*, 299–312. [[CrossRef](#)]
24. Bazai, N.A.; Cui, P.; Liu, D.; Carling, P.A.; Wang, H.; Zhang, G.; Li, Y.; Hassan, J. Glacier surging controls glacier lake formation and outburst floods: The example of the Khurdopin Glacier, Karakoram. *Glob. Planet. Change* **2022**, *208*, 103710. [[CrossRef](#)]

25. Friedl, P.; Seehaus, T.; Braun, M. Global time series and temporal mosaics of glacier surface velocities derived from Sentinel-1 data. *Earth Syst. Sci. Data* **2021**, *13*, 4653–4675. [[CrossRef](#)]
26. Paul, F.; Bolch, T.; Kääb, A.; Nagler, T.; Nuth, C.; Scharrer, K.; Shepherd, A.; Strozzi, T.; Ticconi, F.; Bhambri, R.; et al. The glaciers climate change initiative: Methods for creating glacier area, elevation change and velocity products. *Remote Sens. Environ.* **2015**, *162*, 408–426. [[CrossRef](#)]
27. Bhambri, R.; Hewitt, K.; Kawishwar, P.; Kumar, A.; Verma, A.; Snehmani, Tiwari, S.; Misra, A. Ice-dams, outburst floods, and movement heterogeneity of glaciers, Karakoram. *Glob. Planet. Change* **2019**, *180*, 100–116. [[CrossRef](#)]
28. Haemmig, C.; Huss, M.; Keusen, H.; Hess, J.; Wegmüller, U.; Ao, Z.; Kulubayi, W. Hazard assessment of glacial lake outburst floods from Kyagar glacier, Karakoram mountains, China. *Ann. Glaciol.* **2014**, *55*, 34–44. [[CrossRef](#)]
29. Hewitt, K.; Liu, J. Ice-Dammed Lakes and Outburst Floods, Karakoram Himalaya: Historical Perspectives on Emerging Threats. *Phys. Geogr.* **2010**, *31*, 528–551. [[CrossRef](#)]
30. Round, V.; Leinss, S.; Huss, M.; Haemmig, C.; Hajnsek, I. Surge dynamics and lake outbursts of Kyagar Glacier, Karakoram. *Cryosphere* **2017**, *11*, 723–739. [[CrossRef](#)]
31. Gardner, A.S.; Moholdt, G.; Scambos, T.; Fahnestock, M.; Ligtenberg, S.; van den Broeke, M.; Nilsson, J. Increased West Antarctic and unchanged East Antarctic ice discharge over the last 7 years. *Cryosphere* **2018**, *12*, 521–547. [[CrossRef](#)]
32. Krieger, G.; Moreira, A.; Fiedler, H.; Hajnsek, I.; Werner, M.; Younis, M.; Zink, M. TanDEM-X: A Satellite Formation for High-Resolution SAR Interferometry. *IEEE T Geosci. Remote* **2007**, *45*, 3317–3341. [[CrossRef](#)]
33. van Zyl, J.J. The Shuttle Radar Topography Mission (SRTM): A breakthrough in remote sensing of topography. *Acta Astronaut.* **2001**, *48*, 559–565. [[CrossRef](#)]
34. Hersbach, H.; Bell, B.; Berrisford, P.; Hirahara, S.; Horányi, A.; Muñoz-Sabater, J.; Nicolas, J.; Peubey, C.; Radu, R.; Schepers, D.; et al. The ERA5 global reanalysis. *Q. J. R. Meteorol. Soc.* **2020**, *146*, 1999–2049. [[CrossRef](#)]
35. Guo, W.; Liu, S.; Xu, J.; Wu, L.; Shangguan, D.; Yao, X.; Wei, J.; Bao, W.; Yu, P.; Liu, Q.; et al. The second Chinese glacier inventory: Data, methods and results. *J. Glaciol.* **2015**, *61*, 357–372. [[CrossRef](#)]
36. Zhang, D.; Yao, X.; Duan, H.; Liu, S.; Guo, W.; Sun, M.; Li, D. A new automatic approach for extracting glacier centerlines based on Euclidean allocation. *Cryosphere* **2021**, *15*, 1955–1973. [[CrossRef](#)]
37. Neckel, N.; Braun, A.; Kropáček, J.; Hochschild, V. Recent mass balance of the Purogangri Ice Cap, central Tibetan Plateau, by means of differential X-band SAR interferometry. *Cryosphere* **2013**, *7*, 1623–1633. [[CrossRef](#)]
38. Nuth, C.; Kääb, A. Co-registration and bias corrections of satellite elevation data sets for quantifying glacier thickness change. *Cryosphere* **2011**, *5*, 271–290. [[CrossRef](#)]
39. Guo, W.Q.; Liu, S.Y.; Wei, J.F.; Bao, W.J. The 2008/09 surge of central Yulinchuan glacier, northern Tibetan Plateau, as monitored by remote sensing. *Ann. Glaciol.* **2013**, *54*, 299–310. [[CrossRef](#)]
40. Paul, F.; Barrand, N.E.; Baumann, S.; Berthier, E.; Bolch, T.; Casey, K.; Frey, H.; Joshi, S.P.; Kononov, V.; Le Bris, R.; et al. On the accuracy of glacier outlines derived from remote-sensing data. *Ann. Glaciol.* **2013**, *54*, 171–182. [[CrossRef](#)]
41. Dehecq, A.; Gourmelen, N.; Gardner, A.S.; Brun, F.; Goldberg, D.; Nienow, P.W.; Berthier, E.; Vincent, C.; Wagnon, P.; Trouvé, E. Twenty-first century glacier slowdown driven by mass loss in High Mountain Asia. *Nat. Geosci.* **2018**, *12*, 22–27. [[CrossRef](#)]
42. Fischer, M.; Huss, M.; Hoelzle, M. Surface elevation and mass changes of all Swiss glaciers 1980–2010. *Cryosphere* **2015**, *9*, 525–540. [[CrossRef](#)]
43. Rolstad, C.; Haug, T.; Denby, B. Spatially integrated geodetic glacier mass balance and its uncertainty based on geostatistical analysis: Application to the western Svartisen ice cap, Norway. *J. Glaciol.* **2009**, *55*, 666–680. [[CrossRef](#)]
44. Gardelle, J.; Berthier, E.; Arnaud, Y. Slight mass gain of Karakoram glaciers in the early twenty-first century. *Nat. Geosci.* **2012**, *5*, 322–325. [[CrossRef](#)]
45. Zhang, M.; Chen, F.; Tian, B.; Liang, D.; Yang, A. Characterization of Kyagar Glacier and Lake Outburst Floods in 2018 Based on Time-Series Sentinel-1A Data. *Water* **2020**, *12*, 184. [[CrossRef](#)]
46. Mukherjee, K.; Bolch, T.; Goerlich, F.; Kutuzov, S.; Osmonov, A.; Pieczonka, T.; Shesterova, I. Surge-Type Glaciers in the Tien Shan (Central Asia). *Arct. Antarct. Alp. Res.* **2018**, *49*, 147–171. [[CrossRef](#)]
47. Leclercq, P.W.; Kääb, A.; Altena, B. Brief communication: Detection of glacier surge activity using cloud computing of Sentinel-1 radar data. *Cryosphere* **2021**, *15*, 4901–4907. [[CrossRef](#)]
48. Gardelle, J.; Berthier, E.; Arnaud, Y. Impact of resolution and radar penetration on glacier elevation changes computed from DEM differencing. *J. Glaciol.* **2012**, *58*, 419–422. [[CrossRef](#)]
49. Björnsson, H. Hydrological characteristics of the drainage system beneath a surging glacier. *Nature* **1998**, *395*, 771–774. [[CrossRef](#)]
50. Lv, M.; Guo, H.; Lu, X.; Liu, G.; Yan, S.; Ruan, Z.; Ding, Y.; Quincey, D.J. Characterizing the behaviour of surge- and non-surge-type glaciers in the Kingata Mountains, eastern Pamir, from 1999 to 2016. *Cryosphere* **2019**, *13*, 219–236. [[CrossRef](#)]
51. Björnsson, H.; Pálsson, F.; Sigurdsson, O.; Flowers, G.E. Surges of glaciers in Iceland. *Ann. Glaciol.* **2003**, *36*, 82–90. [[CrossRef](#)]
52. Eisen, O.; Harrison, W.D.; Raymond, C.F.; Echelmeyer, K.A.; Bender, G.A.; Gorda, J.L.D. Variegated Glacier, Alaska, USA: A century of surges. *J. Glaciol.* **2005**, *51*, 399–406. [[CrossRef](#)]
53. Dowdeswell, J.A.; Hamilton, G.S.; Hagen, J.O. The duration of the active phase on surge-type glaciers contrasts between Svalbard and other regions. *J. Glaciol.* **1991**, *37*, 388–400. [[CrossRef](#)]
54. Striberger, J.; Björck, S.; Benediktsson, I.O.; Snowball, I.; Uvo, C.B.; Ingólfsson, O.; Kjaer, K.H. Climatic control of the surge periodicity of an Icelandic outlet glacier. *J. Quat. Sci.* **2011**, *26*, 561–565. [[CrossRef](#)]

55. Dowdeswell, J.A.; Hodgkins, R.; Nuttall, A.M.; Hagen, J.O.; Hamilton, G.S. Mass-Balance Change as a Control on the Frequency and Occurrence of Glacier Surges in Svalbard, Norwegian High Arctic. *Geophys. Res. Lett.* **1995**, *22*, 2909–2912. [[CrossRef](#)]
56. Hoinkes, H.C. Surges of the Vernagtferner in the Ötztal Alps since 1599. *Can. J. Earth Sci.* **1969**, *6*, 853–861. [[CrossRef](#)]
57. Farinotti, D.; Immerzeel, W.W.; de Kok, R.; Quincey, D.J.; Dehecq, A. Manifestations and mechanisms of the Karakoram glacier Anomaly. *Nat. Geosci.* **2020**, *13*, 8–16. [[CrossRef](#)]
58. Wu, K.; Liu, S.; Jiang, Z.; Zhu, Y.; Xie, F.; Gao, Y.; Yi, Y.; Tahir, A.A.; Muhammad, S. Surging Dynamics of Glaciers in the Hunza Valley under an Equilibrium Mass State since 1990. *Remote Sens.* **2020**, *12*, 2922. [[CrossRef](#)]
59. Steiner, J.F.; Kraaijenbrink, P.D.A.; Jiduc, S.G.; Immerzeel, W.W. Brief communication: The Khurdopin glacier surge revisited—Extreme flow velocities and formation of a dammed lake in 2017. *Cryosphere* **2018**, *12*, 95–101. [[CrossRef](#)]
60. Bhambri, R.; Watson, C.S.; Hewitt, K.; Haritashya, U.K.; Kargel, J.S.; Pratap Shahi, A.; Chand, P.; Kumar, A.; Verma, A.; Govil, H. The hazardous 2017–2019 surge and river damming by Shispare Glacier, Karakoram. *Sci. Rep.* **2020**, *10*, 4685. [[CrossRef](#)]
61. Paul, F.; Piermattei, L.; Treichler, D.; Gilbert, L.; Girod, L.; Käab, A.; Libert, L.; Nagler, T.; Strozzi, T.; Wuite, J. Three different glacier surges at a spot: What satellites observe and what not. *Cryosphere* **2022**, *16*, 2505–2526. [[CrossRef](#)]

Disclaimer/Publisher’s Note: The statements, opinions and data contained in all publications are solely those of the individual author(s) and contributor(s) and not of MDPI and/or the editor(s). MDPI and/or the editor(s) disclaim responsibility for any injury to people or property resulting from any ideas, methods, instructions or products referred to in the content.